Draft version November 6, 2017
Typeset using LaTeX **twocolumn** style in AASTeX61

NO TIME FOR DEAD TIME - USE THE FOURIER AMPLITUDE DIFFERENCES TO NORMALIZE DEAD TIME-AFFECTED PERIODOGRAMS

Matteo Bachetti[1] and Daniela Huppenkothen[2,3]

[1] *INAF-Osservatorio Astronomico di Cagliari, via della Scienza 5, I-09047 Selargius (CA)*
[2] *Center for Data Science, New York University, 60 5h Avenue, 7th Floor, New York, NY 10003*
[3] *Center for Cosmology and Particle Physics, Department of Physics, New York University, 4 Washington Place, New York, NY 10003, USA*

(Received XXXX; Revised XXXX; Accepted November 6, 2017)

Submitted to ApJL

ABSTRACT

Dead time affects many of the instruments used in X-ray astronomy, by producing a strong distortion in power density spectra. This can make it difficult to model the aperiodic variability of the source or look for quasi-periodic oscillations. Whereas in some instruments a simple a-priori correction for dead time-affected power spectra is possible, this is not the case for others such as *NuSTAR*, where the dead time is non-constant and long ($\sim$2.5 ms). Bachetti et al. (2015) suggested the cospectrum obtained from light curves of independent detectors within the same instrument as a possible way out, but this solution has always only been a partial one: the measured rms was still affected by dead time, because the width of the power distribution of the cospectrum was modulated by dead time in a frequency-dependent way.

In this Letter we suggest a new, powerful method to normalize cospectra and, with some caveats, even power density spectra. Our approach uses the difference of the Fourier amplitudes from two independent detectors to characterize and filter out the effect of dead time. This method is crucially important for the accurate modelling of periodograms derived from instruments affected by dead time on board current missions like *NuSTAR* and *Astrosat*, but also future missions such as *IXPE*.

Keywords: X-rays: binaries — X-rays: general — methods: data analysis — methods: statistical

Corresponding author: Matteo Bachetti
bachetti@oa-cagliari.inaf.it

1. INTRODUCTION

Dead time is an unavoidable and common issue of photon-counting instruments. It is the time t_d that the instrument takes to process an event and be ready for the next event. In most current astronomical photon-counting X-ray missions, dead time is of the *non-paralyzable* kind, meaning that the instrument does not accept new events during dead time, avoiding a complete lock of the instrument if the incident rate of photons is higher than $1/t_d$. Being roughly energy-independent, dead time is not usually an issue for spectroscopy, as it only affects the maximum rate of photons that can be recorded, so it basically only increases the observing time needed for high quality spectra. For timing analysis, the effect of dead time is far more problematic. The periodogram, commonly referred to as power density spectrum (PDS)[1], which is the most widely used statistical tool to investigate rapid variability, is heavily distorted by dead time, with a characteristic pattern similar to a damped oscillator. This pattern is stronger for brighter sources, and it is often not possible to disentangle this spectral distortion due to dead time and the broadband noise components characterizing the emission of accreting systems. In the special case where dead time is constant, its shape can be modeled precisely (Zhang et al. 1995; Vikhlinin et al. 1994). However, dead time is often different on an event-to-event basis, and it is not obvious how to model it precisely, also because the information on dead time is often incomplete in the data files distributed by HEASARC[2]. For a more thorough discussion about different dead time behaviors see Zhang et al. (1995).

When using data from missions carrying two or more *identical and independent* detectors like *NuSTAR*, Bachetti et al. (2015) proposed an approach to mitigate instrumental effects like dead time exploiting this redundancy: where in standard analysis, light curves of multiple detectors are summed before Fourier transforming the summed light curve, it is possible to instead Fourier-transform the signal of two independent detectors and combine the Fourier amplitudes in a *cospectrum* – the real part of the cross spectrum – instead of the periodogram. Since dead time is uncorrelated between the two detectors, the resulting powers have a mean white noise level fixed to 0, which resolves the first and most problematic issue created by dead time (see details in Bachetti et al. 2015); however, the resulting powers no longer follow the statistical distribution expected for power spectra, and their probability distribution is frequency-dependent. Whereas a noise cospectrum in the absence of dead time would follow a Laplace distribution (Huppenkothen and Bachetti, sub.), dead time affects the width of the probability distribution for cospectral powers and modulates the measured rms proportionally to the distortion acted on power spectra. In this Letter, we show a method to precisely recover the shape of the power density spectrum by looking at the difference of the Fourier amplitudes of the light curves of two independent detectors. This difference, in fact, contains information on the uncorrelated noise produced by dead time, but not on the source-related signal which is correlated between the two detectors. This allows to disentangle the effects of dead time from those of the source variability.

In Section 2 we briefly describe our data analysis and simulation setup. In Section 3 we show that, in the absence of dead time, the Fourier amplitudes of two independent detectors contain the sum of the correlated signal (the source signal) and uncorrelated noise (detector-related noise), and that their difference eliminates the source part. In Section 4 we show that, in the presence of dead time, the difference of the Fourier amplitude still eliminates the source signal but retains information on dead time effects. In Section 5 we show that this can be used to recover the dead noise-free power spectrum.

2. DATA SIMULATION AND ANALYSIS

All simulated and real data sets in this paper were produced and/or analyzed with a combination of the two Python libraries `stingray`[3] (Huppenkothen et al. 2016) and `HENDRICS` v.`3.0b1` (formerly known as MaLTPyNT; Bachetti 2015), both based on Astropy (Astropy Collaboration et al. 2013).

2.1. *Simulated datasets*

We used the same procedure and algorithms described by Bachetti et al. (2015), Section 4, that we briefly summarize here together with references to the methods and classes of the libraries above where these steps are implemented. The classes in `stingray.simulate` were used to simulate light curves with a given noise profile. These classes use the Timmer & Koenig (1995)

[1] here we will use the term PDS for the actual source power spectrum, and *periodogram* to indicate our estimate of it, or otherwise said, the realization of the "real" power spectrum we observe in the data

[2] Whereas in principle this information could be obtained by using the PRIOR column in the unfiltered event files for some missions, the live time given in this column is affected by events that are not recorded in the file, like shield vetos in the case of *NuSTAR*, and the estimate of dead time is necessarily uncertain

[3] The library is under heavy development. For this work we used the version identified by the hash `XXXXXX`

method to create a noise-affected light curve starting from a given power spectral shape described by a powerlaw index, an `astropy` model or a list of arrays containing the frequency and power of the model spectrum. We then used an acceptance-rejection method to obtain simulated events from these light curves (`stingray.Eventlist.simulate_times()`). Finally, the `hendrics.fake.filter_for_deadtime()` function was used to apply a non-paralyzable dead time of 2.5 ms to the simulated event lists. For more details on the simulated data sets, see also Section 5 and the available Jupyter notebooks[4] (for a description of Jupyter notebooks, see Kluyver et al. 2016).

2.2. *Cyg X-1 NuSTAR dataset*

We tested the method also on real data of several bright sources observed by *NuSTAR*. As an example, we report here one such test done on *NuSTAR* data of the black hole binary Cyg X-1 together with the steps to reproduce our analysis, using the linked Jupyter notebook if needed. We downloaded the observation directory of *NuSTAR* ObsID 30001011009 (UT 2014-10-04) from the HEASARC using the custom `heasarc_pipelines` package (Bachetti et al., ASCL identifier requested). Equivalently, this download can be done using the online tools provided by HEASARC (e.g. `xamin`). Starting from the standard cleaned science event files distributed by HEASARC, we applied a barycenter correction using the FTOOL `barycorr` shipped with HEASOFT 6.21 with the clock correction file n. 71 from the *NuSTAR* CALDB. We selected photons in a region of $50''$around the nominal position of Cyg X-1 using the FTOOL `fselect`.[5]. We used the scripts contained in `HENDRICS` to load the event lists for the two detectors FPMA and FPMB, calibrate them to translate the PI channels into energy values, and produced light curves with photons from 3 to 79 keV and binned with uniform time bins of $1/4096 \sim 2.44 \cdot 10^{-4}$ sec[6].

3. ON THE DIFFERENCE OF FOURIER AMPLITUDES

Let us consider two identical and independent detectors observing the same variable source, producing independent time series $\mathbf{x} = \{x_k\}_{k=1}^{N}$ and $\mathbf{y} = \{y_k\}_{k=1}^{N}$. For a stochastic process (e.g. $1/\nu$-type red noise), the Fourier amplitudes will vary as a function of $N_{\rm phot}P(\nu)/4$, where $P(\nu)$ is the shape of the power spectrum underlying the stochastic process, and $N_{\rm phot}$ denotes the number of photons in a light curve. If the two detectors observe the same source simultaneously, the amplitudes and phases of the stochastic process will be shared among $\mathbf{x}$ and $\mathbf{y}$, while each light curve will be affected *independently* by both the photon counting noise in the detector, as well as the dead time process. The resulting Fourier amplitudes will be of the form

$$\begin{aligned} A_{xj} &= A_{xsj} + A_{xdj} + A_{xnj} \\ B_{xj} &= B_{xsj} + B_{xdj} + B_{xnj}\,, \end{aligned} \tag{1}$$

where A_{xsj} and B_{xsj} denote the real and imaginary components of the signal power in the Fourier amplitudes, A_{xdj} and B_{xdj} denote the variance introduced by dead time, and A_{xnj} and B_{xnj} similarly denote the white noise components in the Fourier amplitudes. For a large enough number of data points N, the Fourier amplitudes A_{xj} and B_{xj} will be composed of a sum of three independent random normal variables, with $A_{xsj} \sim \mathcal{N}(0, \sigma_{sj}^2)$, $A_{xdj} \sim \mathcal{N}(0, \sigma_{dj}^2)$ and $A_{xnj} \sim \mathcal{N}(0, \sigma_n^2)$, where $\sigma_{sj}^2 = \sigma_s^2(\nu) = N_{\rm phot}P(\nu)/4$ is given by the (Leahy-normalized, Leahy et al. 1983) power spectrum of the underlying stochastic process, $P_j = P(\nu_j)$, σ_{dj}^2 is an unknown, frequency-dependent variance introduced by dead time, and $N_{\rm phot} = \sum_{k=1}^{N} x_k$ is the integrated flux in the light curve. We also have $\sigma_n^2 = N_{\rm phot}/2$, and hence the combined distributions become

$$\begin{aligned} A_{xj} &\sim \mathcal{N}(0, \sigma_{sj}^2 + \sigma_{dj}^2 + \sigma_n^2) \\ A_{yj} &\sim \mathcal{N}(0, \sigma_{sj}^2 + \sigma_{dj}^2 + \sigma_n^2)\,. \end{aligned}$$

Similar expressions can be found for A_{yj} and B_{yj}, respectively. It is important to note that $A_{xsj} = A_{ysj}$ and similarly $B_{xsj} = B_{ysj}$, that is, the amplitudes of the stationary noise process will be the same for the Fourier transforms of $\mathbf{x}$ and $\mathbf{y}$, while the components due to dead time and white noise differ between the two time series.

As depicted in Figure 1, the correlation between Fourier amplitudes implies that their difference will be independent of the source-induced variability $P(\nu_j)$ and will again be distributed following a normal distribution

$$A_{xj} - A_{yj} \sim \mathcal{N}(0, 2\sigma_{dj}^2 + 2\sigma_n^2)\,.$$

The difference in Fourier amplitudes effectively separates the frequency-dependent effects of source variability and variability due to detector effects.

[4] https://github.com/matteobachetti/deadtime-paper-II

[5] To use the method on different sources, it is sufficient to download a different ObsID and change the region file containing the position of the source

[6] This procedure uses the scripts `HENreadfile`, `HENcalibrate` and `HENlcurve`, as described at http://hendrics.readthedocs.io/en/master/tutorials/quicklook.html

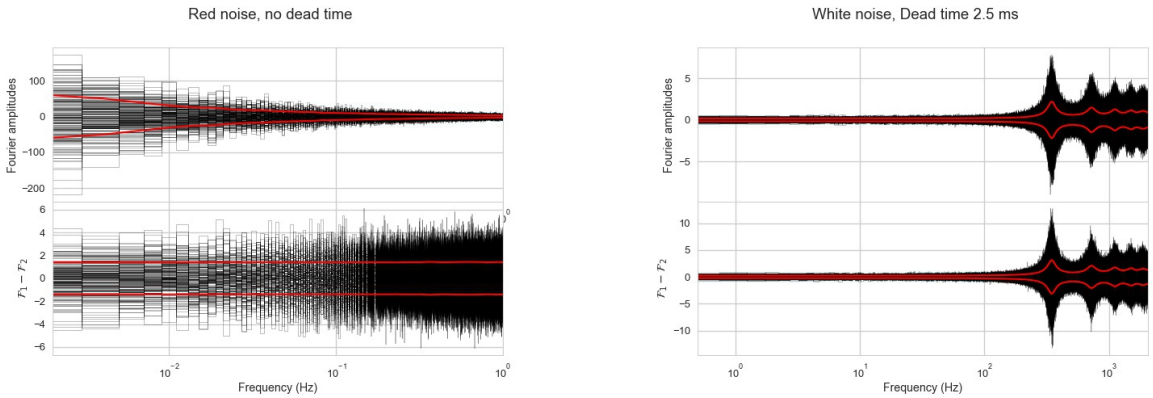

Figure 1. Real Fourier amplitudes obtained by single light curves (top panels) and difference between two realizations of the same source light curve (bottom) in two cases: (Left) Strong $1/f$ red noise and no dead time, calculated over many 500 s segments of the light curve, and (Right) no red noise and strong dead time, calculated over many 5 s segments of the light curve. The choice of different segment length reflects the range of frequencies we want to highlight in the two cases. The red curve gives the frequency-dependent spread of the distributions, measured by the standard deviation of the curves in each frequency bin. As expected, in the first case, the Fourier amplitude follows a power law curve, while the standard deviation of the difference is remarkably stable at all frequencies, as expected by the fact that the Poisson white noise is independent of frequency. In the second case, instead, dead time is frequency dependent and white noise is also affected, so that the difference of Fourier amplitudes is modulated as well.

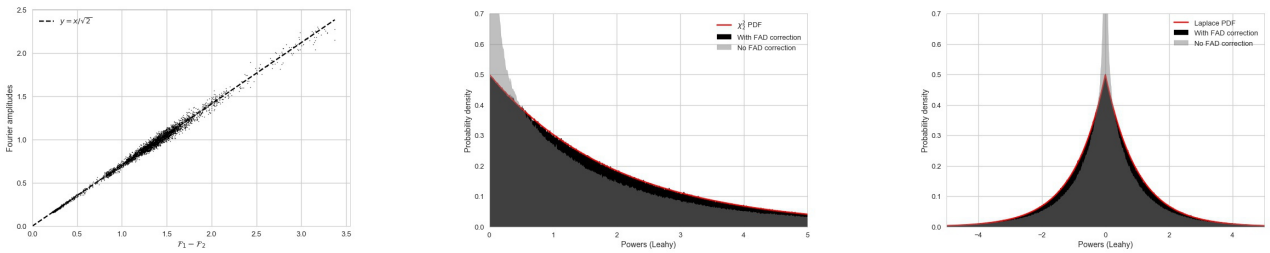

(a) (b) (c)

Figure 2. (a) Scatter distribution of dead time-affected Fourier amplitudes versus the difference of Fourier amplitudes: their relation is clearly linear, with a factor $1/\sqrt{2}$. (b) Distribution of powers in the periodogram, before the FAD correction and after, shown as a histogram. After correction, the powers follow remarkably well the expected χ^2_2 distribution. (c) Same, for the cospectrum. The correct Laplace distribution is followed after FAD correction

4. DEAD TIME-AFFECTED WHITE NOISE

Let us simulate two constant light curves with an incident mean count rate of 400 counts/sec and a dead time of 2.5 ms, as we would expect from two identical detectors observing the same stable X-ray source. This case is illustrated in Figure 1 (right panel). The Fourier amplitudes A_{xj} and A_{yj} of the light curves from the two detectors are heavily distorted by dead time, with the characteristic damped oscillator-like shape (Vikhlinin et al. 1994; Zhang et al. 1995). As laid out in Section 3, the difference of Fourier amplitudes from two independent but identical detectors shows no source variability, but *still shows the same distortion* due to dead time. This gives a clear way to disentangle between source- and dead time-driven variability. By using the difference between the Fourier amplitudes in two detectors, we can in principle renormalize the power spectrum so that only the source variability alters its otherwise flat shape.

As shown in Figure 2 (left panel), the single-channel Fourier amplitudes are proportional to the difference of the Fourier amplitudes in different realizations, with a constant factor $1/\sqrt{2}$. Therefore, we expect that the periodogram will be proportional to the square of the Fourier amplitude difference, divided by 2. Let us try to *divide the power spectrum by a smoothed version of the squared Fourier differences*, and multiply by 2. For smoothing, we used a Gaussian running window with a window width of 50 bins. Given that the initial binning had 50 bins/Hz, this interpolation allows an aggressive smoothing over bins whose y value does not change sig-

nificantly. In general, we recommend smoothing over as many bins as allowed by the shape of the periodogram. In this paper, when not specified we average over the number of bins contained in 1Hz of the spectrum. We call this procedure the **Fourier Amplitude Difference** (hereafter FAD) **correction**.

The correction is depicted in Figure 2, right. Starting from a heavily distorted distribution of the powers, applying the FAD correction reinstates a remarkably correct distribution of powers, following the expected χ^2_2 distribution (Lewin et al. 1988) very closely. Analogously, the corrected cospectrum will follow the expected Laplace distribution. While the original dead time-affected cospectrum had a frequency-dependent modification to the rms level, the FAD-corrected cospectrum gets back to a frequency-independent shape, like in the dead time-free case.

5. TESTING THE FAD CORRECTION ON SIMULATED DATA

We are now ready to verify the last step: is the FAD-corrected power spectrum equivalent (albeit with some loss of sensitivity due to the lower number of photons) to the dead time-free power spectrum? To test this, we produced a number of different synthetic datasets, containing different combinations of QPOs and broadband noise components. We first calculated the periodogram of the dead time-free data. Then, we applied a dead time filter and calculated the power density spectrum and the cospectrum. At this point, we applied the FAD correction, as follows:

1. split the two light curves in segments of 128 to 512 seconds
2. for each pair of light curve segments:
    - calculate the Fourier transform of each channel separately, and then of the summed channels;
    - multiply the Fourier amplitudes by $\sqrt{2/N_{ph}}$ in order to obtain Leahy-normalized periodograms;
    - subtract the Fourier amplitudes of the two channels between them and obtain the Fourier Amplitude Difference (FAD);
    - *smooth* the FAD using a Gaussian-window interpolation with a width of 1-2 seconds;
    - use the separated single-channel and summed Fourier amplitudes to calculate the periodograms;
    - use the Fourier amplitudes from channels A and B to calculate the cospectrum;
    - divide all periodograms and the cospectrum by the smoothed and squared FAD, and multiply by 2.

All spectra were then expressed in fractional rms (Belloni & Hasinger 1990; Miyamoto et al. 1991) normalization, where the integral of the fitted spectral components returns directly its fractional rms. In the rms normalization, the values of each point of the periodogram should be consistent between the dead time-free and the FAD-corrected periodograms. We first checked visually that the spectra (white-noise subtracted in the case of periodograms) after FAD correction were all consistent with the dead time-free periodogram. Then, we fitted all spectra with the model which produced the simulated data and checked that the values were always consistent with the input model parameters and the fit on the dead time-free periodogram. Finally, we verified that the total rms of the FAD-corrected spectra was always consistent with the total rms of the dead time-affected cospectrum *times the ratio between incident and detected photons*, using the count rates before and after applying the dead time filter. To calculate this rms, we fitted the spectra with two Lorentzian components, and used their amplitude in the calculation. In this normalization, the amplitude of a Lorentzian gives the total rms squared of the component. For periodograms, the model included also a constant offset to account for the white noise level. An example of this analysis is shown in Figure 3 (upper panel).

The simulations show that the shape of the periodogram is precisely corrected by the FAD procedure *if* the input light curves have the same count rate. However, in real life the two detectors can receive slightly different signals due to slightly different responses, the presence of gaps inside the PSF, etc. Simulating datasets with slightly different light curve mean rates in the two channels, we indeed find that the performance of the FAD correction degrades. The degradation is higher for higher count rates and higher difference between the two channels. Since the exact degradation is dependent on the shape of the periodograms, we recommend to FAD-correct both the periodogram and the cospectrum, and verify visually that the white-noise subtracted periodogram and the cospectrum are consistent. For example, look for bumps or valleys in the white noise-subtracted periodogram that are not present in the cospectrum, and trust the additional signal to noise of the periodogram only in the regions where the two are consistent.

6. APPLICATION TO CYG X-1

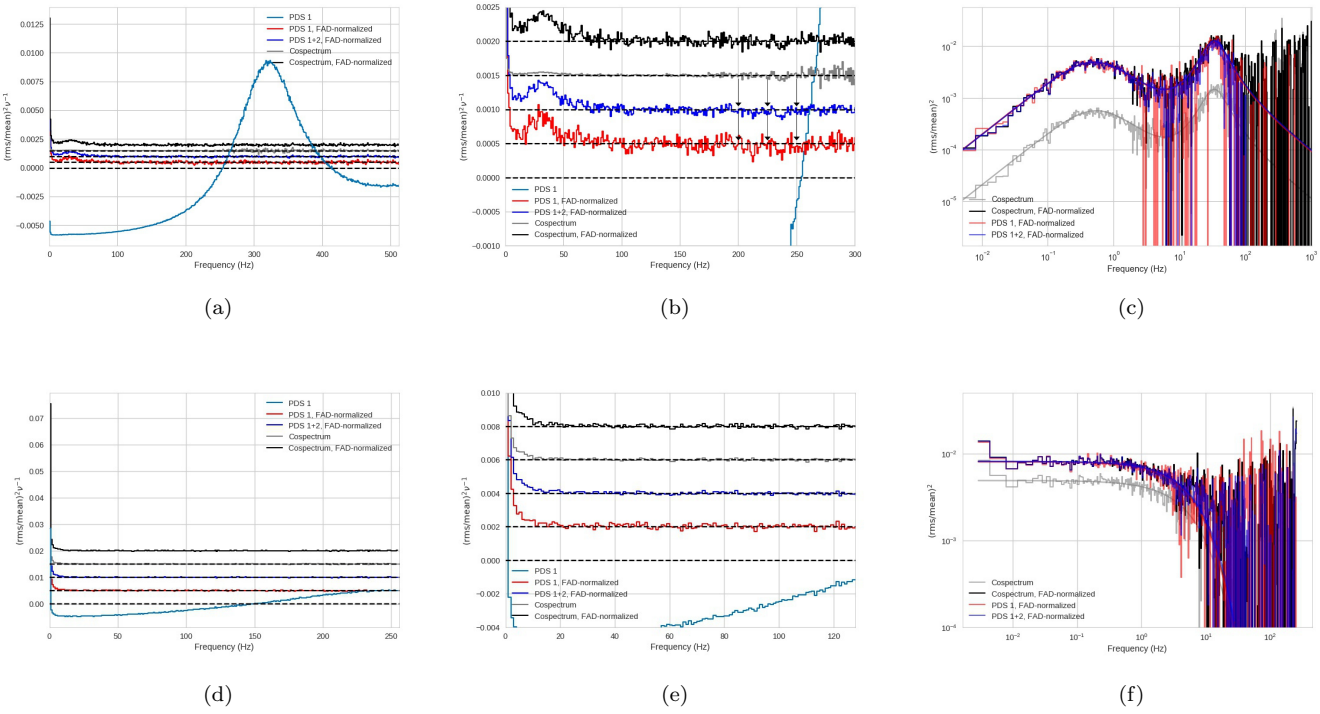

Figure 3. Top: simulated dataset with two strong and broad Lorentzian components, incident count rate ∼810 ct/s, and total rms ∼15% ("detected" after dead time: ∼270 and ∼4% resp.). Bottom: *NuSTAR* observation of the black hole candidate Cyg X-1. (a) and (d): comparison of the distortion of the dead time-affected periodogram with the FAD-corrected periodogram, the dead time-affected and the FAD-corrected cospectrum. The spectra have been shifted vertically for clarity. The shape of the uncorrected periodogram is clearly distorted by dead time. (b) and (e): the FAD correction successfully flattens the periodogram, but there remain a few intervals where the baseline is imperfect, indicated by the arrows. This is due to the flux mismatch between the two detectors (see Section 6). The cospectral powers are always distributed around zero, but dead time changes the width of the resulting distribution, and the FAD correction attenuates the width of the distribution back to the width expected in the dead time-free case (see e.g. (b) for a striking case). Moreover, the source-dominated part of the spectrum also receives a boost, which corrects precisely the measured rms of the source from the "hushing" effect of dead time. (c) and (f): FAD-corrected periodogram and cospectra, plotted in $(\mathrm{rms/mean})^2$ normalization and fitted with two Lorentzian curves (c) and with an exponential cutoff power law (f). The additional gain coming from the FAD normalization is evident by the comparison with the uncorrected cospectrum.

In this Section we apply the FAD correction to a *NuSTAR* observation of Cyg X-1. This source was discovered in the early days of X-ray astronomy (Bowyer et al. 1965) and it is among the best studied X-ray sources in the sky. It is a persistent black hole X-ray binary, alternating soft and hard spectral states with distinct timing and spectral features (see, e.g., Grinberg et al. 2013). The observation we analyze here was taken during the source's soft state, that is characterized by a non-thermal X-ray spectrum, stable radio jets and, what matters the most here, distinct aperiodic variability that is well fitted by an exponential cutoff power law with index ∼ 1 (see, e.g., Gilfanov et al. 2000). We followed the procedure described in Section 5, dividing the light curves in 512-s segments and smoothing the squared FAD with a Gaussian window of 1-s width (512 bins). The results are shown in Figure 3, lower panel for comparison with the simulations.

We fitted the four spectra of Cyg X-1 with an exponential cutoff power law. For periodograms, we added to the models an additive constant to account for the white noise level. In all cases, the estimates returned by the fit were consistent between the different spectra in all but the amplitude parameter of the power law curve. We used this amplitude to calculate the ratios between the rms measured by the deadtime-affected cospectrum and the FAD-corrected spectra. The increase of rms between the dead time-affected cospectrum and the FAD-corrected cospectrum and periodograms is consistent to 2% with the ratio r_{in}/r_{det}, where r_{in} is the incident count rate, and r_{det} is the detected count rate, given by

$$r_{det} = \frac{r_{in}}{1 + t_d r_{in}} \tag{2}$$

(using the standard non-paralyzable dead time formula, where t_d is dead time) which is the drop of rms expected from the effect of dead time (Bachetti et al. 2015).

7. CONCLUSIONS

In this Letter we described a method to correct the normalization of dead time-affected periodograms. This method is valid in principle for 1) correcting the shape of the periodogram, eliminating the well known pattern produced by dead time, and 2) adjusting the white noise standard deviation of periodogram and cospectra to its correct value at all frequencies. In general, we recommend applying the FAD correction to both the periodogram and the cospectrum. The periodogram, if obtained by the sum of the light curves, can yield a higher signal-to-noise ratio. However, the white noise level subtraction is not always very precise due to mismatches in the mean count rate in the two light curves. A comparison with the FAD-corrected cospectrum, to verify visually the white noise subtraction, is always recommended. It is important to be reasonably sure of the white noise level of the periodogram, as the white noise subtraction is the most important step when calculating the significance of a given feature in the periodogram (e.g. Barret & Vaughan 2012; Huppenkothen et al. 2017). The cospectrum has the advantage of not requiring white noise level subtraction.

In all cases, we find that the adjustment of the white noise standard deviation in the periodogram and the cospectrum works remarkably well, allowing to make a confident analysis of X-ray variability even in sources where this was precluded until now. This software will be merged into the main repository of `stingray` before publication. A number of jupyter notebooks will also be posted at the address https://github.com/matteobachetti/deadtime-paper-II to reproduce the full analysis plotted in the Figures of this paper, plus more examples of application of these techniques to simulated and real data.

We thank David W. Hogg for useful discussions on the topic of Fourier analysis. MB is supported in part by the Italian Space Agency through agreement ASI-INAF n.2017-12-H.0 and ASI-INFN agreement n.2017-13-H.0. DH is supported by the James Arthur Postdoctoral Fellowship and the Moore-Sloan Data Science Environment at New York University.

REFERENCES

Astropy Collaboration, Robitaille, T. P., Tollerud, E. J., et al. 2013, A&A, 558, A33

Bachetti, M. 2015, Astrophysics Source Code Library, ascl:1502.021

Bachetti, M., Harrison, F. A., Cook, R., et al. 2015, ApJ, 800, 109

Barret, D., & Vaughan, S. 2012, ApJ, 746, 131

Belloni, T., & Hasinger, G. 1990, A&A, 230, 103

Bowyer, S., Byram, E. T., Chubb, T. A., & Friedman, H. 1965, Astronomical Observations from Space Vehicles, 23, 227

Gilfanov, M., Churazov, E., & Revnivtsev, M. 2000, MNRAS, 316, 923

Grinberg, V., Hell, N., Pottschmidt, K., et al. 2013, 554, 88

Huppenkothen, D., Bachetti, M., Stevens, A. L., Migliari, S., & Balm, P. 2016, Stingray: Spectral-timing software, Astrophysics Source Code Library, , , ascl:1608.001

Huppenkothen, D., Younes, G., Ingram, A., et al. 2017, ApJ, 834, 90

Kluyver, T., Ragan-Kelley, B., Pérez, F., et al. 2016, in ELPUB, 87–90

Leahy, D. A., Darbro, W., Elsner, R. F., et al. 1983, ApJ, 266, 160

Lewin, W. H. G., van Paradijs, J., & van der Klis, M. 1988, SSRv, 46, 273

Miyamoto, S., Kimura, K., Kitamoto, S., Dotani, T., & Ebisawa, K. 1991, ApJ, 383, 784

Timmer, J., & Koenig, M. 1995, A&A, 300, 707

Vikhlinin, A., Churazov, E., & Gilfanov, M. 1994, 287, 73

Zhang, W., Jahoda, K., Swank, J. H., Morgan, E. H., & Giles, A. B. 1995, ApJ, 449, 930